Waste Management 133 (2021) 89–98

Contents lists available at ScienceDirect

Waste Management

journal homepage: www.elsevier.com/locate/wasman

Development of a constitutive model for the compaction of recovered polyethylene terephthalate packages

S. Sanchez-Caballero [a,*], M.A. Selles [b], M.A. Peydro [b], H.P. Cherukuri [c]

[a] Institute of Design and Manufacturing, Universitat Politècnica de València, Plaza Ferràndiz i Carbonell, 2, 03801 Alcoy, Spain
[b] Technological Institute of Materials, Universitat Politècnica de València, Plaza Ferràndiz i Carbonell, 2, 03801 Alcoy, Spain
[c] Department of Mechanical Engineering and Engineering Science, Duke Centennial Hall, The University of North Carolina at Charlotte, Charlotte, NC 28223-0001, USA

ARTICLE INFO

Keywords:
Polyethylene terephthalate
PET
Packaging
Recovery
Compaction
Model
Baler

ABSTRACT

To date, PET (polyethylene terephthalate) is the most widely used plastic in packaging and also one of the most recycled polymers worldwide. However, the high transport costs and stagnated prices of recycled PET undermine recycling process profits. Transport costs can lower through compaction, which is still not a completely well-known process. Due to heterogeneous designs, the output density of the compaction process varies. This poses problems during equipment design, selection or operation processes as recovery costs sharply increase if the required density is not met. In this manuscript, the authors develop a constitutive model for the compaction of recovered PET packaging. This experimentally validated model, based on the elasto-plastic behaviour of PET packages, allows the output density range to be predicted according to the compression pressure during PET compaction. Unlike other generic compaction models that need more than two parameters, this model uses only one and better correlates with the experimental results. Unlike existing generic models, the model parameters have a physical meaning, which allows the influence of different factors on the compaction process to be assessed. Finally as a result of the model analysis, we provide some tips to enhance compaction equipment efficiency.

1. Introduction

PET (polyethylene terephthalate) represents 11.0% of the post-consumer plastic waste in the EU (Alejandro Villanueva, 2014). According to the Annual Survey on the European PET Recycle Industry (PETcore Europe, 2017), the recycling rate of PET bottles in the EU was 58.2% in 2017, and it is expected to reach 90% in 2025. However, recycling PET packages poses some challenges. As the bulk density of packages is usually very low, transportation costs strongly impact the commercial margins of recovered waste sales. Moreover, recovered packaging is often transported several times, first from collection points to selection plants, and then to the plants that recycle separated products.

The fact that the virgin PET price has lowered in the last decade has stagnated recycled PET prices, which is currently at the same level as in 2011, but transportation costs have progressively risen ever since (16% in the USA). According to the "Improving Recycling Markets" report (OECD, 2006), the cost of collecting PET packages and transporting them to recovery plants represents 35.9% of the total cost of this material's recovery process. Furthermore, the costs of compaction and transportation to recycling points respectively represent 6.4% and 5.1%, and amount to nearly half the overall recovery costs. The last EU report about recycling costs (RDCEnvironment and Pira, 2003) also indicates similar values.

Waste is usually compressed to increase its bulk density to lower transportation costs. A smaller volume depends on the subsequent processes that waste undergoes. The volume of the waste taken from collection points to separation facilities is reduced between one half and one third, but not much more because it would hinder the manual or automatic selection processes that are subsequently carried out.

After waste separation, the refused waste volume is reduced mostly to lower the landfill cost. In this way, the most usual density values fall within 230–370 kg/m^3 (OECD, 2006), depending on transportation to either recovery or recycling plants. In the latter case, the density that saturates the maximum semitrailer truck capacity, the vehicle mostly widely used to transport these materials, is around 400 kg/m^3. Therefore, it is most important that this density is at least achieved during the compaction process because otherwise the truck's load capacity will not

* Corresponding author.
E-mail address: sasanca@dimm.upv.es (S. Sanchez-Caballero).

https://doi.org/10.1016/j.wasman.2021.07.028
Received 18 October 2020; Received in revised form 15 July 2021; Accepted 19 July 2021

be taken advantage of, which will make the recovery costs of this waste much more expensive.

Then the heterogeneity of the material comes into play which, due to different package designs, materials and compaction directions, leads to heterogeneous mechanical behaviour. This poses a design problem: the force required to perform compaction is not uniform because it depends on all these factors. Occasionally, the required density is not achieved due to lack of compaction force. This involves having to unpack bales and compress them again to accomplish the appropriate density. To solve this problem, it is necessary to analyse the influential factors in the compaction process to find possible solutions for it.

To date, no studies have been published about the compression behaviour of recovered PET packages. Existing studies focus on the compaction of dust, biomass and municipal solid waste (MSW). Remarkably, none approaches PET packaging behaviour. Thus the need to study the PET compaction process. Table 1 broadly compares currently existing models for many materials, such as alfalfa, wheat, oat, powders, ashes (Kim and Prezzi, 2008), hay, barley straw, MSW, among others.

The following works employ some of the models shown in Table 1 to fit experimental results to different materials:

Adapa et al. (2002) carry out several tests with alfalfa grinds by applying pressures between 16 and 141 MPa. The results of these experiments are fitted using the Panelli and Filho (2001), Heckel (1961), Walker (1923), Jones (1962) and Cooper and Eaton (1962) models, which conclude that Cooper and Eaton (1962) model gives a better fit for low humidity contents (8–9%), while the Heckel (1961) and Panelli and Filho (2001) models work better with higher contents (13–14%).

Denny (2002) makes a theoretical comparison between the models in the works by Heckel (1961), Kawakita and Ludde (1971), and prove that Heckel's model is a generalisation of Kawakita's model.

Mani et al. (2004) perform several essays with wheat and barley straws, corn stover and switchgrass using pressures between 31.08 and 136.77 MPa to obtain output densities from 733 to 1,179 kg/m^3. The results of these experiments are fitted to the equations in Heckel (1961), Cooper and Eaton (1962), and Kawakita and Ludde (1971). They conclude that the equation in Heckel (1961) does not properly fit the experiments. However, the model in Cooper and Eaton (1962) works quite well and that in Kawakita and Ludde (1971) adequately works.

Shaw and Tabil (2005) run several tests with peat moss, wheat straw, oat hulls and flax shives at pressures of 145 MPa and obtain output densities between 1,300 and 1,400 kg/m^3. They use the equations in Walker (1923), Jones (1962), Cooper and Eaton (1962), Kawakita and Ludde (1971) to fit the results of these experiments. They conclude that the last one better fits the experimental results.

Emami and Tabil (2007) make fit comparisons of a series of experiments with the models in Walker (1923), Jones (1962), Barbosa-Canovas et al. (1987), Cooper and Eaton (1962), Kawakita and Ludde (1971) applied to chickpea flour compaction. They conclude that the model of Cooper and Eaton (1962) is the closest one to the experimental results when this material is used.

Adapa et al. (2009) employ four agricultural biomass types (barley, canola, oat, wheat straw) to which they apply pressures up to 140 MPa and obtain densities up to 1,484 kg/m^3. Afterwards, the authors fit the data with the models of Jones (1962), Heckel (1961), Cooper and Eaton (1962), Kawakita and Ludde (1971) and Panelli and Filho (2001). They conclude that the model of Kawakita and Ludde (1971) is the only one suitable one at these pressures because of its very low correlation with the others.

Nona et al. (2014) followed the Faborode and O'Callaghan (1986) method to fit a series of experiments performed with straw and hay by applying pressures of 0.05 MPa with output densities of 140 kg/m^3. The work does not focus on analysing the pressure-density relation, but on studying the relaxation phenomenon.

Table 1
Pressure (p) vs output density (ρ) or compression ratio ($r = \rho/\rho_0$) fitting expressions.

Material	Max. pressure [MPa]	Density [kg/m^3]	Equation	Empirical constants	Reference
Metal powders	–	–	$r^{-1} = a_1 - K_1 \log p$	a_1, K_1	Walker (1923)
Wheat, oat, alfalfa	200	1500	$p = c(\rho - \rho_0)^m$	c, m	Mewes (1958)
Hay straw	34.5	400	$p = Ke^{m\rho}$	m, K	Butler (1958)
Powder	150	–	$\log\frac{1}{1-r} = mp + n$	m, n	Heckel (1961)
Metal powder	–	–	$\log\rho = m\log p + b$	m, b	Jones (1962)
Ceramic & biomass	–	–	$\frac{\rho_0 - \rho}{\rho_0 - \rho_{max}} = Ae^{-B/p} + Ce^{-D/p}$	A, B, C, D	Cooper and Eaton (1962)
Hay	20.0	1,400	$p = e^{C_0 + C_1 W} + C_2 + C_3 W$	C_0, C_1, C_2, C_3	Busse (1963)
Vegetable stalks	–	–	$p = \frac{C}{a}(e^{a(\rho-\rho_0)} - 1)$	a, C	Osobov (1967)
Powder	700	–	$1 - r = \frac{a_1 a_2 p}{1 + a_2 p}$	a_1, a_2	Kawakita and Ludde (1971)
Barley straw	74.0	400	$p = 1.2{\cdot}10^{-5}\rho^2$	–	O'Dogherty and Wheeler (1984)
		⩾400	$\log p = 2.26{\cdot}10^{-3}(\log\rho)^4 - 2.32$	–	
Alfalfa	–	1415	$\frac{\rho_{max} - \rho}{\rho_{max} - \rho_0} = e^{-p/K}$	K	Bilanski et al. (1985)
Straw	–	–	$p = C\rho^m$	C, m	Bilanski et al. (1985)
Barley straw	54.5	1327	$p = \frac{K_0}{b}(e^{b(r-1)} - 1)$	K_0, b	Faborode and O'Callaghan (1986)
Wheat, rye, corn flour	1462	–	$r - 1 = a\log_{10} p + b$	a, b	Barbosa-Canovas et al. (1987)
Barley straw	34.5	640	$p = A_0 e^{B_0\rho}$	A_0, B_0	O'Dogherty (1989)
Rice,barley & wheat	100	1400	$\rho = \rho_0 + (A_0 + B_0 p)(1 - e^{Cp})$	A_0, B_0, C	Ferrero et al. (1991)
Alfalfa wafers	–	–	$p = K_1 \log[1 - K_2(\gamma_s - \gamma_{\rho_0})]$	K_1, K_2	Watts and Bilanski (1991)
Powders	–	–	$\log\frac{\rho}{\rho_{max}} = \log\frac{\rho_0}{\rho_{max}} - kp - b\sqrt{p}$	k, b	Shapiro and Sonnergaard (1993)
Coir pith	0.416	400	$p = A_0 + B_0\rho + C\rho^2$	A_0, B_0, C	Viswanathan and Gothandapani (1999)
Powder	1000	–	$\log\frac{1}{1-r} = a\sqrt{p} + b$	a, b	Panelli and Filho (2001)
Landfill MSW	0.5	1200	$\rho = ap^b$	a, b	Dixon et al. (2005)
Paper & cardboard	10	550	$\rho = a\log p + b$	a, b	Gado et al. (2014)

Stoltz et al. (2010) perform a series of experiments with MSW by working at maximum pressures of 0.3 MPa. They obtain output densities of 1,697 kg/m^3, and show only the correlation graphics between both parameters, but no fit equation.

Ramaiah et al. (2017) measure the mechanical compressibility and shear strength of MSW collected from different locations in the Ghazipur and Okhla dumps, both located in Delhi, by considering pressures up to 0.3 MPa. The correlation between vertical strain and pressure is shown in several graphics with no numerical fitting.

Thus no previous work has dealt with the compaction of recovered PET waste, and many existing models have been used to fit a wide variety of materials (Agranat and Perminov, 2020; Nguyen et al., 2020; Davis et al., 2019; Rodriguez-Delgado et al., 2019). Based on the comparison of previous works, it can be deduced that each model's suitability does not depend so much on the material type, but on the applied compaction pressures. With recovered PET, the maximum pressure of the commercial compaction machines does not exceed values of 1.3 MPa. For example, the strongest baler (29 N Series) of American Baler (2021) exerts a pressure of 1.29 MPa, the one (CD-30X43) of International Baler Corporation (2021) does so at 1.26 MPa and, finally, that (HSM VK 15020) of HSM GmbH + Co. KG (2021) does so at 1.24 MPa. These pressures are noticeably lower to those used in previously described compaction models.

Moreover, the compaction of such waste markedly differs from the compaction processes seen in previous works, which is fundamentally due to the heterogeneity of waste PET bottles (WPB) (geometry and orientation), their stiffness variability, which depends on the direction of the compaction force and the of WPB, and the high porosity (volume of void per total volume) of WPB. Furthermore, PET displays visco-elastic-plastic mechanical behaviour insofar as compression behaviour can also be influenced by compaction speed.

The empirical nature of these works does not allow us to determine the importance of the different factors ruling PET compression process behaviour. Besides, it is not possible to predict the model parameters without carrying out some experiments. The fact that a specific model of the recovered PET's behaviour is lacking often entails the inefficient design of recovery and compaction equipment.

The objective of this work is to analyse the basis of PET packaging behaviour under compression conditions to understand the mechanism of this process. Given this objective, and from the behaviour observed in FEM simulations, we developed a theoretical model that we later used to fit the results obtained in the experimental assays. Knowledge about the compaction process of such waste will not only improve compaction equipment design efficiency, but will also help to develop other pre-treatments to perform a better process.

2. Constitutive models for the visco-elasto-plastic behaviour of PET

To date PET packages are made of PET in its pure form as virgin PET (Alvarado Chacon et al. (2020), Awaja and Pavel (2005)), which may be blended with small amounts of recycled PET (rPET). Previous works, such as that by (Chilton et al., 2010), conduct on a full-scale bottle manufacturing plant, find that the maximum rPET proportion that can be used is 5%. Higher proportions of rPET-produced bottles contain specks of black material, which is unacceptable for bottle manufacturers. Other works like (Alvarado Chacon et al., 2020) study the effect of higher rPET concentrations on optical and mechanical properties, and find a direct linear relation between rPET concentration and haziness/particle contamination. When blended, rPET has to be melted and is formed into pellets with the same physical dimensions and degree of crystallinity as virgin PET. The mechanical properties of virgin PET and rPET blends can be considered similar because the degree of crystallinity is similar and no increases in rPET concentrations are foreseeable in the future.

Previous works have shown that PET exhibits visco-elasto-plastic behaviour. Ghorbel (2008) report a viscoplastic model and propose a yield criterion for PET, among other thermoplastics, based on a combination of the Modified Von Mises Criterion (MMC) and a Drucker-Prager Criterion. Unfortunately, these criteria do not match the experimental shear stress values obtained upon yielding semicrystalline polymers like PET. These authors only conduct cyclic tensile-compressive tests for PA12.

Hirsekorn et al. (2009) and Hirsekorn et al. (2011) develop a visco-elasto-plastic model for PET films based on multilayer polymeric films. The visco-elastic strain is modelled using a generalised Kevin-Voigt model in the form of prony series. The viscoplastic strain is modelled in the same way as the visco-elastic strain, but the strain recovery of elements is not allowed. For each visco-elastic element, another visco-plastic one is added with the same retardation time. These authors run several creep tests to determine the visco-elasto-plastic model parameters.

Li et al. (2010) study the viscoplastic behaviour of PET in large strains. According to the previous works of Zaroulis and Boyce (1997) and Dupaix and Boyce (2005), PET exhibits strain hardening for large strains, which is dependent on not only the strain, but also on the strain rate. These authors use the Cowper and Symonds model Cowper and Symonds (1957) according to Eqs. (1)–(3) to predict the yield strength and to describe rate-dependent yield behaviour. They carry out tensile tests at different strain rates until break and determine the elastic-plastic parameters of the Cowper and Symonds model.

$$\sigma_y = \sigma_o(\varepsilon_p) f(\dot{\varepsilon}_p) \tag{1}$$

$$\sigma_0(\varepsilon_p) = \sigma_0 + K\varepsilon_p^n \tag{2}$$

$$f(\dot{\varepsilon}_p) = 1 + (\dot{\varepsilon}_p/D)^{1/q} \tag{3}$$

where σ_y is the equivalent yield stress, $\sigma_0(\varepsilon_p)$ is the yield stress at the zero plastic strain, ε_p and $\dot{\varepsilon}_p$ are the true plastic strain and strain rate, respectively, $f(\dot{\varepsilon}_p)$ represents viscoplastic behaviour, K is the strain-hardening coefficient, n is the strain-hardening exponent, D and q are strain-rate hardening coefficients.

Shil'ko et al. (2014) and Shil'ko et al. (2015) model the thermovisco-elastic behaviour of PET and polytetrafluoroethylene filled with PET particles, respectively, with a generalised Maxwell model in the form of prony series according to Eq. (4). They run several relaxation tests with PET specimens to determine this model's thermovisco-elastic parameters.

$$\sigma = \sigma_{\text{deviatoric}} + \sigma_{\text{volumetric}} = \int_0^t 2G(t-\tau)\frac{de}{d\tau}d\tau + \delta\int_0^t K(t-\tau)\frac{d\varepsilon}{d\tau}d\tau \tag{4}$$

where σ is the stress tensor, e and ε are respectively the deviatoric and volumetric components of the strain, $G(t)$ and $K(t)$ are the deviatoric and bulk relaxation modulus of the material, t is the real time and τ is the elapsed time.

Volumetric stress is neglected compared to deviatoric stress according to Starovoitov and Naghiyev (2012) and the observations of Shil'ko et al. (2015). Function $G(t-\tau)$ is approximated using a prony series of two terms according to Eq. (5).

$$G(t-\tau) = G_0\left[\alpha_\infty^G + \sum_{i=1}^{n_G}\alpha_i^G \exp\left(-\frac{t-\tau}{\tau_i^G}\right)\right] \tag{5}$$

where G_0 is the shear modulus at t = 0 and $\alpha_i = G_i/G_0, \tau_i^G$ is the relaxation time for each prony series component, $\alpha_\infty^G = 1 - \sum_{i=1}^{n}\alpha_i$.

Berezvai and Kossa (2020) report a visco-elastic-viscoplastic constitutive model for microcellular thermoplastic foam. The model comprises a Maxwell-type non-linear visco-elastic branch and an elastic-plastic network, and is generally known as a two-layer viscoplastic model (TLVP). The material's elastic behaviour is modelled by linear isotropic

elasticity, which is represented by an elastic modulus (E_P) on the elastic-plastic branch and a visco-elastic modulus (E_V) on the visco-elastic one. Non-linear viscous behaviour is modelled with two creep power-law models: the time-hardening power-law shown in Eq. (6); a strain-hardening power-law according to Eq. (7). The elastic-plastic branch is modelled using the Von Mises yield criterion combined with a linear isotropic hardening rule. Several dynamic mechanical analyses (DMA) tests are performed to fit the constitutive model's parameters.

$$\dot{\bar{\varepsilon}}_{cr} = Aq^n t^m \tag{6}$$

$$\dot{\bar{\varepsilon}}_{cr} = (Aq^n[(m+1)\bar{\varepsilon}_{cr}]^m)^{\frac{1}{m+1}} \tag{7}$$

where q is Von Mises stress, $\bar{\varepsilon}_{cr} = \sqrt{2/3\varepsilon_{cr} : \varepsilon_{cr}}$, ε_{cr} is the creep strain tensor, and A, n and m are parameters.

3. Materials and methods

3.1. Finite element model

A FEM simulation of a bottle compression process is carried out to understand the behaviour of PET packages under compression. The chosen packages are: a typical 500 ml soda bottle; typical 500 ml and 2,000 ml water bottles. The CAD models of the three packages are supplied by a manufacturer. Thus both geometry and thickness correspond to real packages. These simulations aim to acquire qualitative knowledge about the influence of the package geometry and compression direction on the compaction process, rather than performing constitutive model parameter estimations. Thus only two different directions, two distinct volumes and two differing geometries are considered.

FEM simulations are made using the "Explicit Dynamics" module of the Ansys Workbench 19 R3 software, which is suitable for predicting complex responses like large material deformations, interactions between bodies or rapidly changing surfaces. This module can remesh the geometry with large deformations and strains. The compression process is modelled in two different directions: axial (along the bottle axis) and radial (perpendicular to the bottle axis).

The finite element model is developed according to the following assumptions: i. bottles are placed inside a box with zero clearance with ideally rigid behaviour; ii. the friction effects of packaging with the walls of the box are not contemplated; iii. one of the sides of the box is opened, and a press plate replaces it to exert pressure on the bottle in the chosen direction. The press plate moves at a constant speed of 15 mm/s. iv. the visco-elastic behaviour of PET is modelled with a Maxwell model in the form of prony series, as shown in Eq. (4), according to the work of Shil'ko et al. (2014) and using the following parameters: $G_0 = 1,376$ MPa; $K = 6,050$ MPa; $\alpha_1^G = 0.34$; $\alpha_2^G = 0.39$; $\tau_1^G = 0.01$ s; $\tau_2^G = 3.48$ s. v. as wide local deformations can be expected, viscoplastic behaviour is modelled with a Cowper and Symonds model according to the work of Li et al. (2010) with Eqs. (1)–(3), and the following parameters: $\sigma_0 = 59.65$ MPa, $K = 352.13$ MPa, $n = 2.11, D = 3.42$ and $q = 1.41$.

Fig. 1 and 2d show the compression process simulations for all the package types and in each direction for a 60% volume reduction. Compression pressure is calculated by dividing the force by the pressing area. The volume reduction ratio is calculated by dividing the volume remaining to be compressed by the initial compression chamber volume. We can see that the pressure required at this point is null for the three bottle types when the force direction is radial. However, the pressure required during axial compression varies from 0.6 to 0.9 MPa due to the

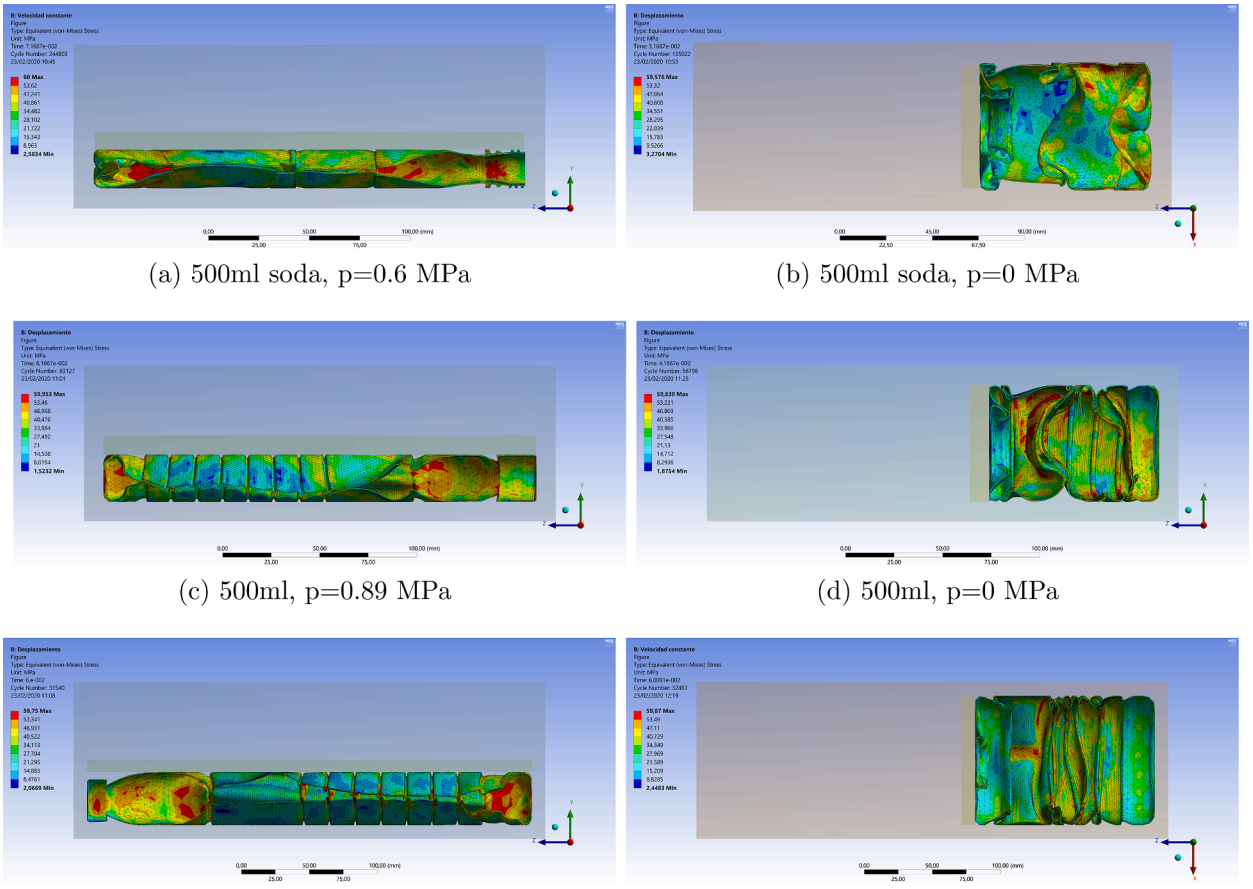

(a) 500ml soda, p=0.6 MPa (b) 500ml soda, p=0 MPa

(c) 500ml, p=0.89 MPa (d) 500ml, p=0 MPa

(e) 2000ml, p=0.33 MPa (f) 2000ml, p=0 MPa

Fig. 1. FEM simulation comparison at 60% volume reduction. Direction: left = radial & right = axial.

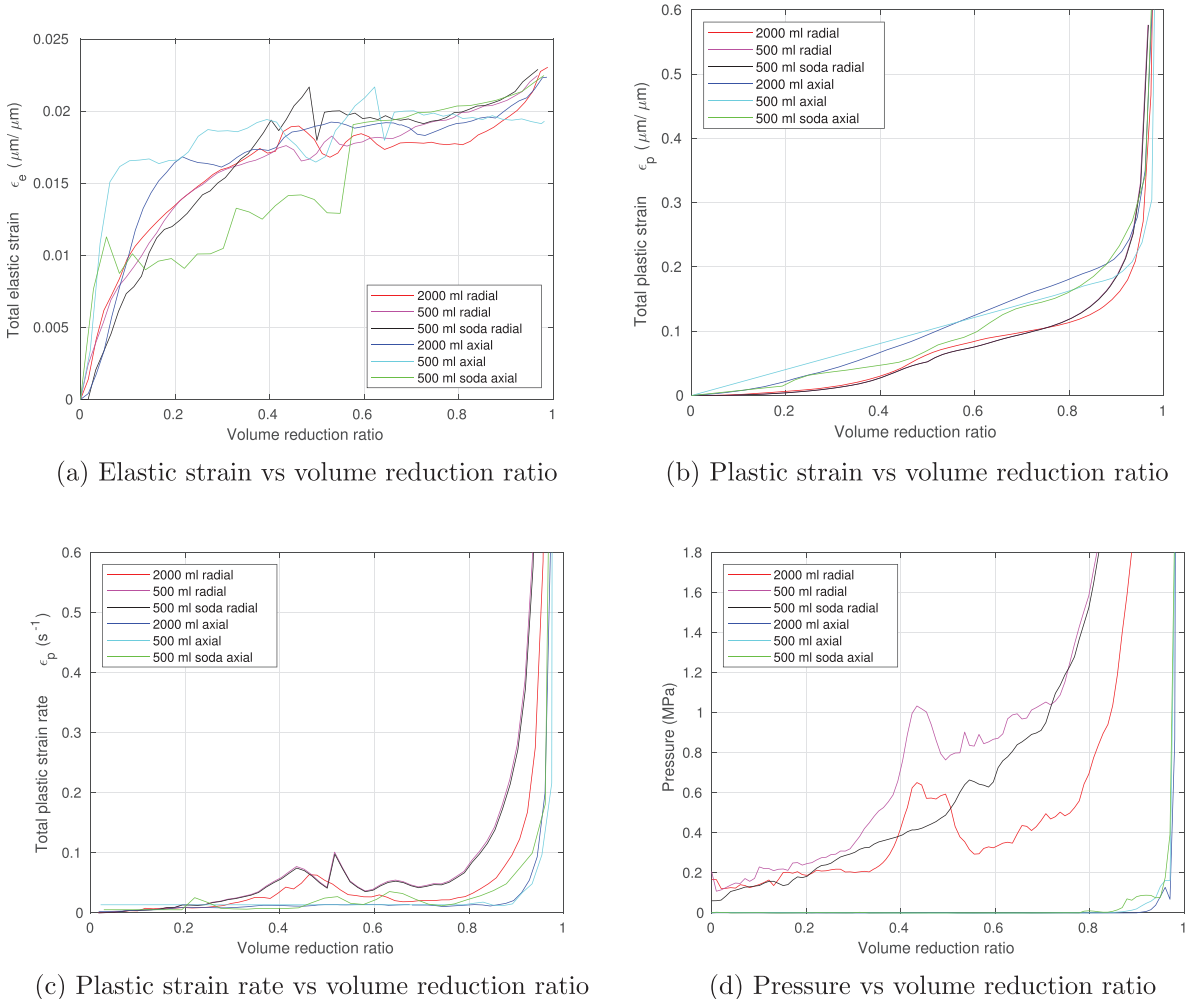

(a) Elastic strain vs volume reduction ratio

(b) Plastic strain vs volume reduction ratio

(c) Plastic strain rate vs volume reduction ratio

(d) Pressure vs volume reduction ratio

Fig. 2. FEM simulations results.

greater bottle stiffness in this direction.

Fig. 2a shows the average elastic strain that provides the mean value over all the elastic strain tensors of the FEM model. This provides us with an indicator of the overall elastic deformation level that the bottle undergoes. The higher the average elastic strain, the more FEM elements that undergo elastic deformation. Elastic strain oscillations are due to bottle stiffness variations (foldings, buckling) during the compaction process. As we can see, the average elastic strain grows to almost 0.024 $\mu m/\mu m$, which corresponds to the yield strain of PET; i.e., around 98% of the volume reduction ratio. Fig. 2b shows the average plastic strain that represents the overall plastic deformation level that the bottle undergoes. Similarly, the higher the average plastic strain, the more FEM elements that undergo plastic deformation. As shown, the plastic strain trend is similar in all cases, with quasilinear growth up to the 80% volume reduction. From this point onwards, the strain exponentially increases. The plastic strain rate (see Fig. 2c) is related to the material's plastic hardening effect. Rate oscillations are due to bottle stiffness variations (foldings, buckling) during the compaction process. Plastic strain behaviour is similar in the same bottle orientation. It shows an almost null value for the axially pressed bottles and is slightly higher in the radial pressing direction. When we analyse the evolution of the pressure required throughout the compression process shown in Fig. 2d, we see how the required pressure is almost zero in the axial direction up to an 80% volume reduction. In the radial direction, a sustained increase continues from the beginning. The two humps seen in the 500 ml bottles correspond to the bottleneck deformation.

From these results, we can deduce that the compression process generates mainly a plastic deformation of bottles with two clearly differentiated parts. A first section up to a volumetric reduction of approximately 80%, where air is expelled from inside the pressing chamber, plasticity grows steadily and the strain rate is low. And a second section where the inner walls of the bottle touch one another at different points, and the compaction process comes closer to the uniaxial compression of the raw material as the number of contact points increases. In this stage, plasticity and its rate exponentially grow, which lead to a rapidly rising compaction pressure. Because of this exponential correlation, the minor error in the computation of displacements inherent to any FEM simulation is amplified when determining compaction pressure. Therefore, FEM predictions will be less accurate for volume reduction ratios beyond 80%. Of the three package types, the soda bottle and the 500 ml water bottle display similar behaviour, with greater stiffness than the 2,000 ml package when radially pressed. According to Figs. 2b, c and d, pressure rises as the plastic strain does with a clear plastic hardening effect. In contrast when cylinders are axially compressed, the required pressure does not increase much with rising pressure, which implies barely any or no plastic hardening effect. The plastic strain rate has no significant effect on the material's hardening in the first section because, even for the maximum point value of 0.1, its influence is only 8% on hardening according to Eq. 3.

3.2. Constitutive model development

With the FEM simulation results, a theoretical model of the material's behaviour during the pressing process is developed based on the

following assumptions: isotropic behaviour; a non-linear stress/strain ratio; showing hardening behaviour. Based on these hypotheses, an elasto-visco-plastic solid mechanical analogue is created to model the PET bottles deformation inside the compression chamber.

The elasto-viscoplastic model is created by connecting a strain-hardening spring element, a dashpot element and a friction element in parallel (Fig. 3).

The total stress (σ) in the elasto-viscoplastic model is the sum of the stress in the spring element (σ_s), the dashpot element (σ_d) and the friction element (σ_f). The total stress is exerted by the ram force on the press area, which is known as specific compression pressure p:

$$\sigma = \sigma_s + \sigma_d + \sigma_f = p \tag{8}$$

With the strain-hardening spring element, the spring comprises an elastic component and a strain-hardening component. This approach differs to the conventional approach used in other models for biomass compaction (Peleg (1983, 1989)), which employ two parallel springs. However, it is reported by other authors for powder compaction (Cunningham et al. (2004)) and biomass (Kaliyan and Morey (2009)).

Elastic component behaviour is modelled as:

$$\varepsilon_e = \left(\mathcal{H}[\sigma_y - \sigma_s]\sigma_s + \mathcal{H}[\sigma_s - \sigma_y]\sigma_y\right)E^{-1} \tag{9}$$

where $\mathcal{H}[\sigma]$ is the Heaviside step function, while E is the elastic modulus of WPB and represents the stress to elastic natural strain ε_e ratio of WPB, and σ_y is the yield stress of the WPB.

Strain-hardening component behaviour is modelled as:

$$\varepsilon_p = \mathcal{H}[\sigma_s - \sigma_y]\left(\frac{\sigma_s}{K}\right)^{1/n} = \mathcal{H}[\sigma_s - \sigma_y]K^{-1/n}\sigma_s^{1/n} \tag{10}$$

where ϵ_p is the natural plastic strain, K is the strength coefficient or plastic modulus of WPB and n is the strain-hardening exponent.

The total natural strain of the strain-hardening spring element can be calculated as the sum of the elastic and plastic strains:

$$\varepsilon = \varepsilon_e + \varepsilon_p = \mathcal{H}[\sigma_y - \sigma_s]E^{-1}\sigma_s + \mathcal{H}[\sigma_s - \sigma_y]\left(E^{-1}\sigma_y + K^{-1/n}\sigma_s^{1/n}\right) \tag{11}$$

The dashpot element is modelled as:

$$\sigma_d = \eta\frac{d\varepsilon}{dt} \tag{12}$$

Finally, the frictional stress (σ_f) in the friction element represents stress due to the friction between bottles and the press chamber walls. This frictional stress is proportional to the spring force according to Cunningham et al. (2004):

$$\sigma_f = \sigma_T - \sigma_B = \ln\left(\frac{\sigma_T}{\sigma_B}\right)\sigma_s = c_f\sigma_s \tag{13}$$

where σ_T is the stress on the press plate (top) and σ_B is the stress at the bottom of the press chamber. According to Cunningham et al. (2004), the ratio between them both (c_f) can be considered constant throughout the compaction process.

In this way, from Eq. (8) the stress in the spring element can be written as:

$$\sigma_s = \frac{p - \sigma_d}{1 + c_f} = k_s(p - \sigma_d) \tag{14}$$

The natural strain is measured according to Eq. (15), which falls in line with other authors like Kaliyan and Morey (2009), Cunningham et al. (2004).

$$\varepsilon = \ln\left(\frac{H_0}{H_0 - \Delta H}\right) \tag{15}$$

where H_0 is the initial compaction chamber length at t = 0, and ΔH is the change of its length or ram displacement.

By computing the first derivative of Eq. (11) in relation to the stress in springs, and by considering that the natural strain is defined as $d\varepsilon = -dz/z = -dV/V$ (negative sign denotes compression), we obtain the differential equation that rules the compaction process:

$$\frac{d\varepsilon}{d\sigma_s} = -\frac{dV/V}{d\sigma_s} = E^{-1} + \mathcal{H}[\sigma_s - \sigma_y]\frac{\sigma_s^{-1+1/n}}{nK^{1/n}} \tag{16}$$

From Eq. (16), it can be concluded that any increment in strain can lead to rising stress non-linearly if stress overcomes the yield point, unlike other models like that proposed by Faborode and O'Callaghan (1986), where this relation is constant. This observation is in accordance with

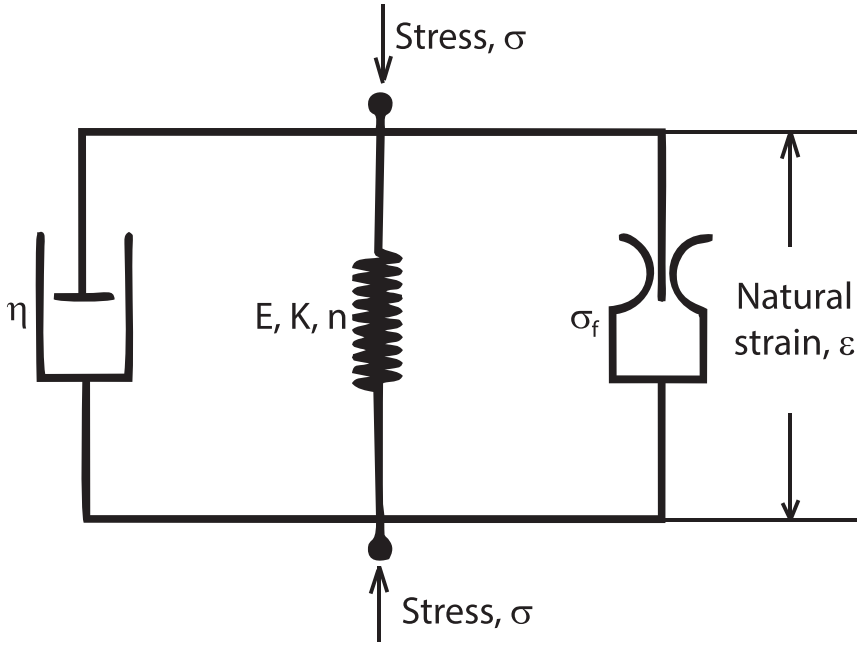

Fig. 3. Elasto-visco-plastic constitutive model.

the empirical results obtained during compression tests.

By rearranging the terms in Eq. (16), we obtain a first-order homogeneous differential equation.

$$dV + V\left(E^{-1} + \mathcal{H}[\sigma_s - \sigma_y]\frac{\sigma_s^{-1+1/n}}{nK^{1/n}}\right)d\sigma_s = 0 \tag{17}$$

By considering boundary condition $V(\sigma_s = 0) = V_0$, and replacing σ_s according to Eq. (14), we obtain:

$$V = V_0 e^{-E^{-1}k_s(p-\sigma_d)-K^{-1/n}((k_s(p-\sigma_d))^{1/n}-\sigma_y^{1/n})\mathcal{H}[k_s(p-\sigma_d)-\sigma_y]} \tag{18}$$

As the mass inside the compression chamber remains constant, the output density (ρ) can be obtained from the input one (ρ_0) according to the specific pressing pressure from Eq. (18) as follows:

$$\rho = \rho_0 e^{E^{-1}k_s(p-\sigma_d)+K^{-1/n}((k_s(p-\sigma_d))^{1/n}-\sigma_y^{1/n})\mathcal{H}[k_s(p-\sigma_d)-\sigma_y]} \tag{19}$$

Eq. (19) shows that increased density is fundamentally due to two components: an elastic ($e^{E^{-1}k_s(p-\sigma_d)}$) and a plastic component ($e^{\sigma_y^{1/n}\mathcal{H}[k_s(p-\sigma_d)-\sigma_y]}$), where the elastic and plastic moduli, and the hardening exponent, define which component contributes the most to increased density.

From Eq. (18) and 19, the compression ratio can be determined. It represents the volume (or density) variation during the pressing process, and is one of the fundamental parameters for designing and selecting compaction equipment:

$$r = \frac{\rho}{\rho_0} = \frac{V_0}{V} = e^{E^{-1}k_s(p-\sigma_d)+K^{-1/n}((k_s(p-\sigma_d))^{1/n}-\sigma_y^{1/n})\mathcal{H}[k_s(p-\sigma_d)-\sigma_y]} \tag{20}$$

3.3. PET packages pressing

In order to experimentally validate the theoretical model, a series of tests is performed. Tests are run at room temperature (20 °C) on a vertical press capable of exercising a force of 100 kN on a 250x250 mm area, which entails a maximum specific pressing pressure of 1.6 MPa. As commercial compaction machines for packages can yield a compaction pressure from 0.8 to 1.4 MPa, our tests can be considered representative of existing compaction machines. The compression chamber height is 297.9 mm.

Force is measured with an U3-100 kN force sensor at 0.05% precision (brand HBM). Displacement is measured by a displacement sensor (ASM model WS1.1-750-R1K-L10) at 0.1% precision. Data are recorded by an MGCPLUS acquisition system by HBM at a sample rate of 10 Hz. The test speed remains constant at 15 mm/s.

During the experiments, different package volumes are used and pressed in both directions: axial and radial. Table 2 summarises the used materials and test conditions.

After running tests, the results are fitted to both the developed model and the different pre-existing models using the `fit` function of Matlab R2019b.

4. Results and discussion

4.1. Constitutive model correlation with FEM simulations

Having developed the theoretical model, the model's constitutive parameters are fitted to the results obtained with the FEM simulations to obtain the correlation among them. The theoretical model presents a high correlation with the FEM results at low compaction pressures. The fit values and their goodness are seen in the first six rows in Table 3.

Fig. 4a shows the comparison between the developed model and the FEM simulation results. It denotes a remarkable difference between radial and axial compactions by exhibiting higher compaction ratios in the axial direction.

According to the FEM model assumptions, the fitting parameters are only valid at low compaction pressures ($p \leqslant 1.6$ MPa) and compaction velocity ($v \leqslant 15$ mm/s).

Table 2
Test summary. Number, volume and weight of the tested packages.

Test name	Individual volume [ml]	Total Vol. [ml]	Weight [g]	Direction
PET01	5x1,500 + 500 + 330 + 350	8,680	235	radial
PET02	3x1,500 + 2x500 + 350 + 5x330	7,500	263	radial
PET03	2,000 + 3x1,500 + 750 + 350 + 5x330	9,250	265	radial
PET04	2x2,000 + 3x1,500 + 3x330	9,490	221	radial
PET05	2,000 + 4x1,500 + 2x500 + 2x350 + 2x330	10,360	260	radial
PET06	5x1,500 + 350 + 4x330	9,170	226	axial
PET07	2,000 + 2x1,500 + 4x350 + 12x330	10,360	325	axial
PET08	500 + 5x350 + 17x330	7,860	334	radial
PET09	1,500 + 3x350 + 24x330	10,470	428	axial
PET10	2,000 + 3x1,500 + 2x500 + 2x350	8,200	233	axial
PET11	16x500 + 8x330	10,640	488	axial
PET12	34x330	11,220	512	axial
PET13	4x1,500 + 4x500 + 4x330	9,320	405	axial
PET14	6x1,500 + 4x330	10,320	382	axial
PET15	16x500 + 6x350	10,100	447	axial
PET16	5x1,500 + 4x350	8,900	409	axial
PET17	4x1,500 + 12x330	9,960	436	axial
PET18	4x350 + 26x330	9,980	421	axial
PET19	18x500	9,000	399	axial
PET20	16x500 + 6x330	9,980	426	axial

4.2. Constitutive model correlation with the experimental results

Fig. 4b shows the results of the experimental tests and the obtained fitting curves. A wide dispersion appears in the output density function of the specific compaction pressure. This dispersion is due to a wide typology of packages with different geometries, thicknesses and orientations when pressed, which provides a wide range of stiffness (E,K) and strain-hardening exponents (n) values.

Table 3 shows the results of the fitting parameters of the different tests. The mean coefficient of friction (c_r) computed from fitting parameter k_s agrees with the coefficient of friction between PET and steel reported by Buick et al. (2005), Samyn et al. (2006). As we can see, dashpot stress comes close to zero, so viscous stress element σ_d can be neglected in Eqs. (18)–(20). This agrees with what is observed in the FEM results described in Section 3.1, where the plastic strain rate has a negligible effect. The correlation of the experimental results with the theoretical model is $R^2 > 0.98$. As noted, the tests carried out in the radial direction (PET01 to PET05 and PET08) attain a lower output density than the axial ones. According to the constitutive model assumptions, the fitting parameters are valid only at low compaction pressures ($p \leqslant 1.6$ MPa) because the compression tests are carried out up to this value. Moreover, the constitutive model cannot be extrapolated to processes that require high pressure, such as pelleting, because air is expelled at higher pressure and bottles can begin to behave like the raw material. This means that a totally different material model needs to be applied. Finally due to the visco-elastic and viscoplastic behaviour of PET, the test results and fit values depend on the test speed and are, therefore, only valid for speeds close to 15 mm/s. Given the temperature dependence of PET, the results are only valid at around 20 °C, which is the testing temperature.

As seen in Table 3, the elastic modulus is quite high. So the elastic component barely impacts increased density as $e^{E^{-1}k_s(p-\sigma_d)} \approx 1$. Furthermore, as the yield stress (σ_y) is very low, increased density due to elastic deformation is negligible. This observation corresponds to the FEM analysis results in Section 3.1 where the average elastic strain

Table 3
Fitting parameters (PET).

Test name	ρ_o [kg/m^3]	E [MPa]	K [Pa]	k_s [–]	n [–]	σ_y [Pa]	$\sigma_{d_{max}}$ [Pa]	c_f [–]	R^2 [–]
ax. 500	17.439	4197.71	59.58	0.872	6.936	0.00	9.73	0.146	0.958
ax. 500s	24.101	2206.91	0.38	0.879	9.127	13.85	1.89	0.138	0.986
ax. 2000	11.860	2851.92	0.03	0.838	8.396	0.00	6.67	0.193	0.988
rad.500	17.439	4203.38	371.47	0.800	8.205	1006.18	5.86	0.250	0.985
rad.500s	24.101	4190.15	4603.10	0.800	8.565	1032.25	6.75	0.250	0.953
rad.2000	11.860	2971.23	264.99	0.803	12.574	43.50	3.61	0.246	0.956
PET01	12.966	2689.84	2.97	0.864	8.032	224.56	3.35	0.158	0.984
PET02	14.510	117.83	4643.32	0.801	4.120	249.60	5.75	0.248	1.000
PET03	14.621	2520.58	2.92	0.914	7.672	648.08	8.64	0.095	0.987
PET04	12.193	969.46	2.67	0.864	7.594	490.96	1.99	0.157	0.987
PET05	14.345	100.29	20.82	0.829	6.852	316.63	6.72	0.206	1.000
PET06	12.469	1343.97	1.48	0.832	7.667	265.16	9.02	0.202	0.999
PET07	17.931	1030.31	24.15	0.832	6.628	496.25	1.99	0.202	1.000
PET08	18.428	100.55	2674.62	0.825	4.737	61.43	2.98	0.212	0.986
PET09	23.614	1044.52	22.84	0.861	6.801	857.74	4.97	0.161	0.999
PET10	12.855	687.88	6.22	0.830	6.826	424.31	8.90	0.204	0.998
PET11	26.210	2650.83	173.11	0.834	5.538	2455.38	5.01	0.199	1.000
PET12	27.499	1931.35	14.84	0.849	6.849	1799.40	2.77	0.177	0.990
PET13	21.752	2130.54	13.37	0.865	7.205	221.56	5.34	0.156	0.995
PET14	20.517	2633.32	23.91	0.843	6.855	157.71	5.74	0.186	0.988
PET15	24.008	1284.31	4.79	0.820	7.535	402.48	4.13	0.219	0.991
PET16	21.967	1867.16	5.16	0.844	7.018	1591.04	0.15	0.184	0.996
PET17	23.417	1598.68	4.20	0.830	7.502	606.19	7.03	0.206	0.994
PET18	22.612	2533.91	14.46	0.864	6.337	3658.63	5.07	0.158	0.985
PET19	21.430	1425.03	12.23	0.838	6.548	1722.83	3.81	0.194	0.997
PET20	22.880	1834.05	8.78	0.842	6.939	637.46	0.65	0.188	0.997
Average	19.311	1103.71	14.32	0.850	6.803	778.87	3.59	0.176	0.994

tensor is negligible compared to the average plastic strain one. Accordingly, Eq. (19) can be approximated in a simpler form as:

$$\rho \approx \rho_0 e^{\left(\frac{k_s}{K}p\right)^{1/n}} \tag{21}$$

where $k_s \approx 0.85$ can be considered constant.

In order to determine the possible correlation between the fit parameters, the relation between them is studied. No correlation appears between input density and the other fit parameters, or between the fit parameters with one another, except for the plastic modulus (K) and the strain-hardening exponent (n). However, as shown in Fig. 4,c a clear correlation between the plastic modulus and the strain-hardening exponent appears. In this way, and considering the correlation of K, and n, the developed model only requires one parameter to characterise the material's behaviour. Therefore, tests are run in the axial direction of packages to yield lower exponents, which indicate the material's greater compressibility. Conversely, exponents are higher when pressing in the radial direction. This corresponds to the behaviour observed in both the FEM simulations and tests.

Fig. 4d shows the fitted curves between both extremes of Fig. 4b, along with the average fit, whose fit parameters are observed at the end of Table 3. The average curve represents the limit between the compaction in the axial and radial directions. For an output density from 300 to 400 kg/m^3, compaction pressures are widely dispersed and even require pressures above 1.6 MPa. This value far exceeds existing equipment's current compaction capacity. As a result, the low-density bales have to be undone and reprocessed, with the consequent loss in productivity and a higher compaction process cost.

4.3. Correlation with other pre-existing theoretical models

In order to compare the newly developed theoretical model to other pre-existing models, these models are fitted to obtain the correlation values for each one. Table 4 shows the means and medians of the coefficients of regression R^2 of each model. Most pre-existing models present a good correlation, but they all require from two to four parameters, which are significantly more than the new model. Additionally, the developed model is not merely a mathematical fit to the experimental results, but is based on parameters with physical meaning, such as WPBs' elastic and plastic moduli, and the strain-hardening exponent.

5. Conclusions

This work proposes a mathematical model that allows the compression behaviour of recovered PET packages to be predicted. It is built with theoretical reasoning based on the theory of elasticity, and it fundamentally requires one parameter, plastic modulus K, because the strain-hardening exponent (n) correlates with it.

This work proves that the new model accurately represents the compression behaviour of different packaging types with regression coefficients (R^2) above 0.98. These coefficients are not only better than those obtained by other pre-existing models, but the model needs only one parameter versus the two, three or four parameters that others require. Fundamental parameter K and the remaining derived parameters have a clearly defined physical meaning, which enables their interpretation. Thus it can be stated that the compression behaviour of PET packages is influenced mainly by the compression force direction rather than by a package's stiffness, which derives from its design or volume. As a result of this analysis, compressibility of packages is significantly higher when compressed in the axial direction than in the radial direction. Therefore, compaction equipment's feeding system should ensure that packages are placed in a machine's axial direction, which is not presently the case. Today's feeding systems fill the press chamber without ensuring specific package orientation. An axial orientation can be achieved by feeding the compaction equipment with conveyor belts with crosspieces at a high inclination angle, which allows those bottles not aligned with the crosspiece to fall. In this way, if the belt is placed perpendicularly to the compaction axis, packages mostly fall in the press chamber in line with the press axis.

This change in feeding compaction equipment can double its compaction capacity, while achieving more uniform output density at the same time, and avoiding the low-density problems that occasionally

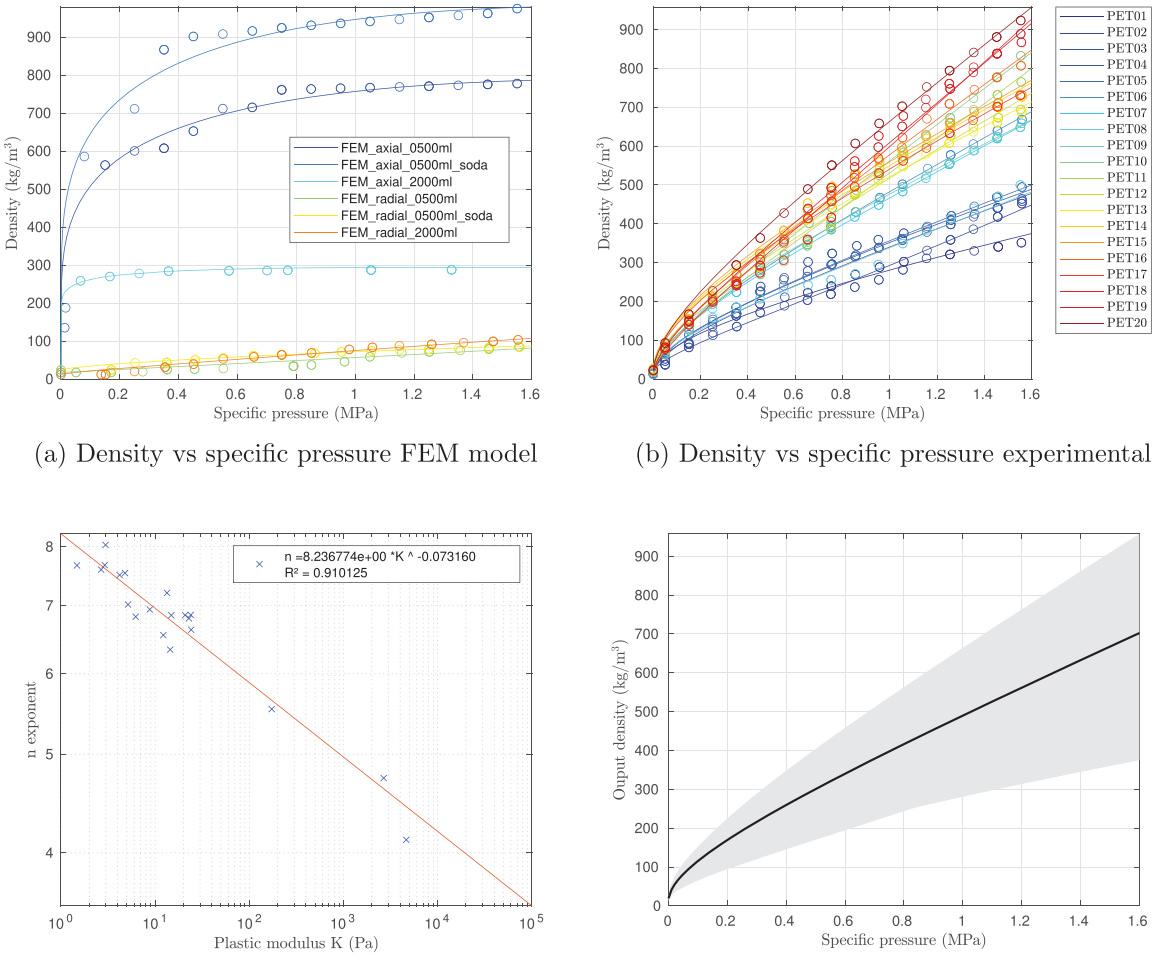

(a) Density vs specific pressure FEM model

(b) Density vs specific pressure experimental

(c) Correlation between the plastic modulus K and the hardening exponent n

(d) Boundaries of model prediction

Fig. 4. Constitutive model fitting results.

Table 4
R^2 regression coefficients of new and previous models.

Model	Parameters	Mean	Median
New	1	0.989	0.995
Walker	2	0.889	0.887
Mewes	2	0.893	0.896
Butler	2	0.841	0.842
Heckel	3	0.846	0.897
Jones	2	0.791	0.793
Busse	4	0.796	0.798
Osobov	2	0.891	0.894
Kawakita	2	0.786	0.791
Bilanski	2	0.991	0.993
Callaghan	2	0.988	0.990
Barbosa	2	0.889	0.887
Ferrero	3	0.795	0.797
Viswanathan	3	0.895	0.897
Dixon	2	0.791	0.793
Gado	2	0.889	0.887
Panelli	2	0.880	0.884

appear in packages.

Finally, this study determines through experiments the relation between the compaction pressure and output density of PET bottles during compaction, and establishes the upper and lower bounds of such behaviour. Based on the assumptions of the constitutive model, and its dependence on compaction conditions, these bounds can be affected mainly by temperature and compaction velocity. These bounds, as well as the constitutive model, are valid only for predicting PET compaction at low pressure.

Declaration of Competing Interest

The authors declare that they have no known competing financial interests or personal relationships that could have appeared to influence the work reported in this paper.

Acknowledgements

Funding for open access charge: CRUE- Universitat Politècnica de València.

References

Adapa, P., Tabil, L., Schoenau, G., 2009. Compression characteristics of selected ground agricultural biomass. Agric. Eng. Int. CIGR Ej. XI. Manuscript 134.

Adapa, P., Tabil, L., Schoenau, G., Crerar, B., Sokhansanj, S., 2002. Compression characteristics of fractionated alfalfa grinds. Powder Handl. Process. 14, 252–259. + 300.

Agranat, V., Perminov, V., 2020. Mathematical modeling of wildland fire initiation and spread. Environ. Model. Softw. 125.

Alejandro Villanueva, P.E., 2014. End-of-waste criteria for waste plastic for conversion. Techreport. European Commission. Joint Research Centre. Institute for Prospective Technological Studies.

Alvarado Chacon, F., Brouwer, M.T., Thoden van Velzen, E.U., 2020. Effect of recycled content and rPET quality on the properties of PET bottles, part i: Optical and mechanical properties. Packaging Technol. Sci. 33, 347–357.
American Baler, 2021. https://americanbaler.com/.
Awaja, F., Pavel, D., 2005. Recycling of PET. Eur. Polymer J. 41, 1453–1477.
Barbosa-Canovas, G., Malave-Lopez, J., Peleg, M., 1987. Density and compressibility of selected food powders mixtures. J. Food Process Eng. 10, 1–19.
Berezvai, S., Kossa, A., 2020. Performance of a parallel viscoelastic-viscoplastic model for a microcellular thermoplastic foam on wide temperature range. Polym. Test. 84, 106395.
Bilanski, W., Graham, V., Hanusiak, J., 1985. Mechanics of bulk forage deformation with application to wafering. Trans. ASAE 28, 697–0702.
Buick, J.M., Chavez-Sagarnaga, J., Zhong, Z., Ooi, J.Y., null Pankaj, Campbell, D.M., Greated, C.A., 2005. Investigation of silo honking: Slip-stick excitation and wall vibration. J. Eng. Mech. 131, 299–307.
Busse, W., 1963. Untersuchungen uber das brikettieren von halmgut (investigation into the wafering of hay and straw). Grundlagen der Landtecbnik 18, 50–57.
Butler, J., 1958. Factors Affecting the Pelleting of Hay. Michigan State University of Agriculture and Applied Science. Department of Agricultural Engineering.
Chilton, T., Burnley, S., Nesaratnam, S., 2010. A life cycle assessment of the closed-loop recycling and thermal recovery of post-consumer PET. Resour. Conserv. Recycl. 54, 1241–1249.
Cooper Jr., A.R., Eaton, L.E., 1962. Compaction behavior of several ceramic powders. J. Am. Ceram. Soc. 45, 97–101.
Cowper, G.R., Symonds, P.S., 1957. Strain-hardening and strain-rate effects in the impact loading of cantilever beams. Technical Report. Brown Univ Providence Ri.
Cunningham, J., Sinka, I., Zavaliangos, A., 2004. Analysis of tablet compaction. I. Characterization of mechanical behavior of powder and powder/tooling friction. J. Pharm. Sci. 93, 2022–2039.
Davis, J., Gebrehiwot, T., Worku, M., Awoke, W., Mihretie, A., Nekorchuk, D., Wimberly, M., 2019. A genetic algorithm for identifying spatially-varying environmental drivers in a malaria time series model. Environ. Model. Softw. 119, 275–284.
Denny, P.J., 2002. Compaction equations: a comparison of the heckel and kawakita equations. Powder Technol. 127, 162–172.
Dixon, N., Russell, D., Jones, V., 2005. Engineering properties of municipal solid waste. Geotext. Geomembr. 23, 205–233.
Dupaix, R.B., Boyce, M.C., 2005. Finite strain behavior of poly(ethylene terephthalate) (PET) and poly(ethylene terephthalate)-glycol (PETg). Polymer 46, 4827–4838.
Emami, S., Tabil, L., 2007. Friction and compression characteristics of chickpea flour and components. Powder Technol. 175, 14–21.
Faborode, M., O'Callaghan, J., 1989. A rheological model for the compaction of fibrous agricultural materials. J. Agric. Eng. Res. 42, 165–178.
Faborode, M.O., O'Callaghan, J.R., 1986. Theoretical analysis of the compression of fibrous agricultural materials. J. Agric. Eng. Res. 35, 175–191.
Ferrero, A., Horabik, J., Molenda, M., 1991. Density-pressure relationship in compaction of straw. Can. Agric. Eng. 33, 107–111.
Gado, I., Ouiminga, S., Daho, T., Yonli, A., Sougoti, M., Koulidiati, J., 2014. Characterization of briquettes coming from compaction of paper and cardboard waste at low and medium pressures. Waste Biomass Valorization 5, 725–731.
Ghorbel, E., 2008. A viscoplastic constitutive model for polymeric materials. Int. J. Plast. 24, 2032–2058.
Heckel, R., 1961. Density-pressure relationship in powder compaction. Trans. Metall. Soc. AIME 221, 671–675.
Hirsekorn, M., Petitjean, F., Deramecourt, A., 2009. A continuous threshold model for the visco-elasto-plastic behavior of PET based multi-layer polymeric films. Mech. Time-Dependent Mater. 14, 25.
Hirsekorn, M., Petitjean, F., Deramecourt, A., 2011. A semi-analytical integration method for the numerical simulation of nonlinear visco-elasto-plastic materials. Mech. Time-Dependent Mater. 15, 139–167.
HSM GmbH + Co. KG, 2021. https://eu.hsm.eu/.
International Baler Corporation, 2021. https://www.intl-baler.com/.
Jones, W.D., 1962. Fundamental principles of powder metallurgy. von w. d. jones, london, edward arnold publishers ltd., 1960, 1032 s., 316 abb., 81 tab., leinen, £ 7 7s net. Mater. Corros. 13, 54.
Kaliyan, N., Morey, R.V., 2009. Constitutive model for densification of corn stover and switchgrass. Biosyst. Eng. 104, 47–63.
Kawakita, K., Ludde, K.H., 1971. Some considerations on powder compression equations. Powder Technol. 4, 61–68.
Kim, B., Prezzi, M., 2008. Evaluation of the mechanical properties of class-f fly ash. Waste Manage. 28, 649–659.
Li, Q., Liu, S.l., Zheng, S.y., 2010. Rate-dependent constitutive model of poly(ethylene terephthalate) for dynamic analysis. J. Zhejiang Univ. Sci. A 11, 811–816.
Mani, S., Tabil, L., Sokhansanj, S., 2004. Evaluation of compaction equations applied to four biomass species. Can. Biosyst. Eng./ Le Genie des biosystems au Canada 46, 3.55–3.61.
Mewes, E., 1958. Zum verhalten von pressgutern in prestopfen (on the behaviour of compressed matter in pressure chambers). andtechnische Forschung 8, 154–164.
Nguyen, V., Dietrich, J., Uniyal, B., 2020. Modeling interbasin groundwater flow in karst areas: Model development, application, and calibration strategy. Environ. Model. Softw. 124.
Nona, K.D., Lenaerts, B., Kayacan, E., Saeys, W., 2014. Bulk compression characteristics of straw and hay. Biosyst. Eng. 118, 194–202.
O'Dogherty, M.J., 1989. A review of the mechanical behaviour of straw when compressed to high densities. J. Agric. Eng. Res. 44, 241–265.
O'Dogherty, M.J., Wheeler, J.A., 1984. Compression of straw to high densities in closed cylindrical dies. J. Agric. Eng. Res. 29, 61–72.
OECD, 2006. Improving Recycling Markets.
Osobov, V.I., 1967. Theoretical principles of compressing fibrous plant materials. Trudy Viskhom, Moscow.
Panelli, R., Filho, F.A., 2001. A study of a new phenomenological compacting equation. Powder Technol. 114, 255–261.
Peleg, K., 1983. A rheological model of nonlinear viscoplastic solids. J. Rheol. 27, 411–431.
PETcore Europe, 2017. ICIS and Petcore Europe PET Recycling Survey 2017. Technical Report. ICIS and Petcore.
Ramaiah, B., Ramana, G., Datta, M., 2017. Mechanical characterization of municipal solid waste from two waste dumps at delhi, india. Waste Manage. 68, 275–291.
RDCEnvironment and Pira, 2003. Evaluation of costs and benefits for the achievement of reuse and recycling targets for the different packaging materials in the frame of the packaging and packaging waste directive 94/62/EC - Final consolidated report. Technical Report. European Commision.
Rodriguez-Delgado, C., Bergillos, R., Iglesias, G., 2019. An artificial neural network model of coastal erosion mitigation through wave farms. Environ. Model. Softw. 119, 390–399.
Samyn, P., Baets, P.D., Schoukens, G., Peteghem, A.V., 2006. Large-scale tests on friction and wear of engineering polymers for material selection in highly loaded sliding systems. Mater. Des. 27, 535–555.
Shapiro, I., Sonnergaard, J., 1993. Compaction of powders x. development of a general compaction equation. Adv. Powder. Metall. Part. Mater. 3, 229–243.
Shaw, M., Tabil, L., 2005. Compression studies of peat moss, wheat straw, oat hulls and flax shives. Powder Handl. Process. 17, 344–350.
Shil'ko, S., Chernous, D., Kropotin, O., Mashkov, Y., 2015. Computational and experimental determination of the viscoelastic parameters of the dispersed-filled polymeric materials. Procedia Eng. 113, 499–505. Oil and gas engineering (OGE-2015) Omsk State Technical University, Omsk, Russian Federation, 25–30 April 2015.
Shil'ko, S.V., Chernous, D.A., Panin, S.V., 2014. Method of determining the thermoviscoelastic parameters of polymers and elastomers. J. Eng. Phys. Thermophys. 87, 984–987.
Starovoitov, E., Naghiyev, F., 2012. Foundations of the Theory of Elasticity, Plasticity, and Viscoelasticity, first ed. Apple Academic Press.
Stoltz, G., Gourc, J.P., Oxarango, L., 2010. Characterisation of the physico-mechanical parameters of msw. Waste Manage. 30, 1439–1449.
Viswanathan, R., Gothandapani, L., 1999. Pressure density relationships and stress relaxation characteristics of coir pith. J. Agric. Eng. Res. 73, 217–225.
Walker, E., 1923. The properties of powders. part vi. the compressibility of powders. Trans. Faraday Soc. 19, 73–82.
Watts, K., Bilanski, W., 1991. Stress relaxation of alfalfa under constant displacement. Trans. ASAE 34, 2491–2504.
Zaroulis, J., Boyce, M., 1997. Temperature, strain rate, and strain state dependence of the evolution in mechanical behaviour and structure of poly(ethylene terephthalate) with finite strain deformation. Polymer 38, 1303–1315.